Geochimica et Cosmochimica Acta 390 (2025) 57–69

Contents lists available at ScienceDirect

Geochimica et Cosmochimica Acta

journal homepage: www.elsevier.com/locate/gca

Controls on the distribution of dissolved Cr in the upper water column of the Atlantic Basin

D. Gilliard [a,*], D.J. Janssen [b,c], N. Schuback [b,d,e], S.L. Jaccard [a,b]

[a] Institute of Earth Sciences (ISTE), University of Lausanne, 1015 Lausanne, Switzerland
[b] Institute of Geological Sciences & Oeschger Centre for Climate Change Research, Baltzerstrasse 1-3, University of Bern, 3012 Bern, Switzerland
[c] Eawag – Swiss Federal Institute of Aquatic Science and Technology (EAWAG), Seestrasse 79, 6047 Kastanienbaum, Switzerland
[d] Swiss Polar, Institute, Rue de l'Industrie 17, 1950 Sion, Switzerland
[e] Chelsea Technologies Ltd., West Molesey KT8 2QZ, UK

ARTICLE INFO

Associate editor: Tim Conway

Keywords:
Chromium
Chromium isotopes
Atlantic Ocean
Water mass mixing

ABSTRACT

Over the last decades, the chromium (Cr) stable isotope system (referred to as $\delta^{53}Cr$) has emerged as a proxy to reconstruct past oxygenation changes in Earth's atmosphere and oceans. Although Cr is a promising paleoproxy, uncertainties remain as to the modern marine Cr cycle, and limited data are yet available in large swaths of the ocean, including the Atlantic Ocean. Here we present dissolved seawater Cr concentrations ([Cr]) and $\delta^{53}Cr$ along a meridional transect from the North to the South Atlantic (AMT 29). Chromium concentrations range from of 2.51 to 3.96 nmol kg^{-1} (n = 68) and $\delta^{53}Cr$ values range from +0.86 ± 0.04 ‰ (2SEM) to +1.20 ± 0.02 ‰ (2SEM) (n = 68). In contrast to data from other ocean basins [Cr] and $\delta^{53}Cr$ show only a weak correlation ($\delta^{53}Cr$ vs. Ln([Cr]) $R^2 = 0.17$), inconsistent with a closed-system Rayleigh distillation model. These results can mainly be explained by horizontal advection and water mass mixing, which our data demonstrate are the dominant processes controlling [Cr] and $\delta^{53}Cr$ distributions throughout much of the Atlantic, while the impact of in situ biogeochemical cycling is comparatively minor. There is, indeed no clear impact of biological productivity nor of dysoxic environments in the (sub)tropical Atlantic on the cycling of Cr along the transect. This is likely explained by insufficiently depleted oxygen concentrations and relatively low biological productivity, resulting in these processes being of secondary importance relative to water mass mixing in shaping the distribution of Cr in the low- to mid-latitude Atlantic Ocean.

1. Introduction

The growing interest in the marine biogeochemical cycle of Cr has largely been spurred by its potential application as a proxy for Earth's oxygenation in the past (e.g., Frei et al., 2009; Reinhard et al., 2014). The foundation of these applications relates to the notion that oxidative weathering on land leads to isotope fractionation, resulting in isotopically heavy Cr transported to the ocean via rivers (e.g., Wei et al., 2020). This distinct isotopic signature can be recorded in marine sediments, and hence sedimentary stable $\delta^{53}Cr$ signals may serve as a proxy of past oxygenation of Earth's atmosphere and oceans (e.g., Frei et al., 2011; Planavsky et al., 2018; Wang et al., 2019; Frei et al., 2021). The robust application of Cr as a proxy in paleoenvironmental studies, however, relies on mechanistic constraints of the multi-facetted processes that regulate $\delta^{53}Cr$ cycling in surface waters as well as the transfer of signals to underlying marine sediments. As such, a thorough understanding of Cr dynamics in the modern ocean is essential to support its application as a paleoproxy.

Seawater [Cr] typically range between 1.2 and 5.6 nmol kg^{-1}, while $\delta^{53}Cr$ values vary between +0.6 ‰ and +1.7 ‰ (Scheiderich et al., 2015; Goring-Harford et al., 2018; Moos and Boyle 2019; Rickli et al., 2019; Nasemann et al., 2020; Janssen et al., 2020, 2021, 2023; Moos et al., 2020; Huang et al., 2021; Baconnais, 2022; Wang et al., 2023a; 2023b). Scheiderich et al., (2015) first reported a tight relationship between dissolved [Cr] and $\delta^{53}Cr$, corresponding to an effective isotope enrichment factor (ε) of approximately −0.8 ± 0.03 ‰ 2SD, and suggested that the isotope fractionation occurring in the ocean was likely driven by a limited number of processes. These processes include biologically-

* Corresponding author.
E-mail addresses: delphine.gilliard@unil.ch (D. Gilliard), david.janssen@eawag.ch (D.J. Janssen), nina.schuback@swisspolar.ch (N. Schuback), samuel.jaccard@unil.ch (S.L. Jaccard).

https://doi.org/10.1016/j.gca.2024.10.017
Received 11 October 2023; Accepted 17 October 2024
Available online 20 October 2024

mediated reduction and associated removal of Cr in surface waters as well as the removal of Cr in oxygen-depleted environments (e.g., Jeandel and Minster 1987; Semeniuk et al., 2016; Janssen et al., 2020, 2021; Pöppelmeier et al., 2021; Huang et al., 2021). Based on vertical profiles reflecting the biological removal of Cr in the photic zone, along with its release (desorption) from sinking particles at depth, Cr can be characterized as a nutrient-type element (e.g., Campbell and Yeats 1981; Jeandel and Minster, 1987; Janssen et al., 2020; 2021; Horner et al., 2021). However, variations in dissolved Cr with depth exhibit a limited gradient compared to other nutrient-type species such as phosphate (PO_4^{3-}), nitrate (NO_3), silicate (Si), iron (Fe), and cadmium (Cd) (e.g., Bruland et al., 2014).

Chromium is predominantly delivered to the ocean via rivers (Bonnand et al., 2013; McClain and Maher 2016; Pöppelmeier et al., 2021) after terrestrial oxidative weathering (Eary and Rai, 1987; D'Arcy et al., 2016). The oceanic flux of Cr via rivers is estimated to amount 2.5 $\times$ 10^8 mol/yr (Pöppelmeier et al., 2021). Chromium has also been shown to diffuse out of pelagic sediments to overlaying abyssal waters (Jeandel and Minster, 1987, Janssen et al., 2021, Bruggmann et al., 2023). The estimated global benthic flux of Cr amounts to ~6 $\times$ 10^8 mol/yr (Pöppelmeier et al., 2021; Steiner et al., 2023), with spatial heterogeneity in different oceanic environments (Shaw et al., 1990;

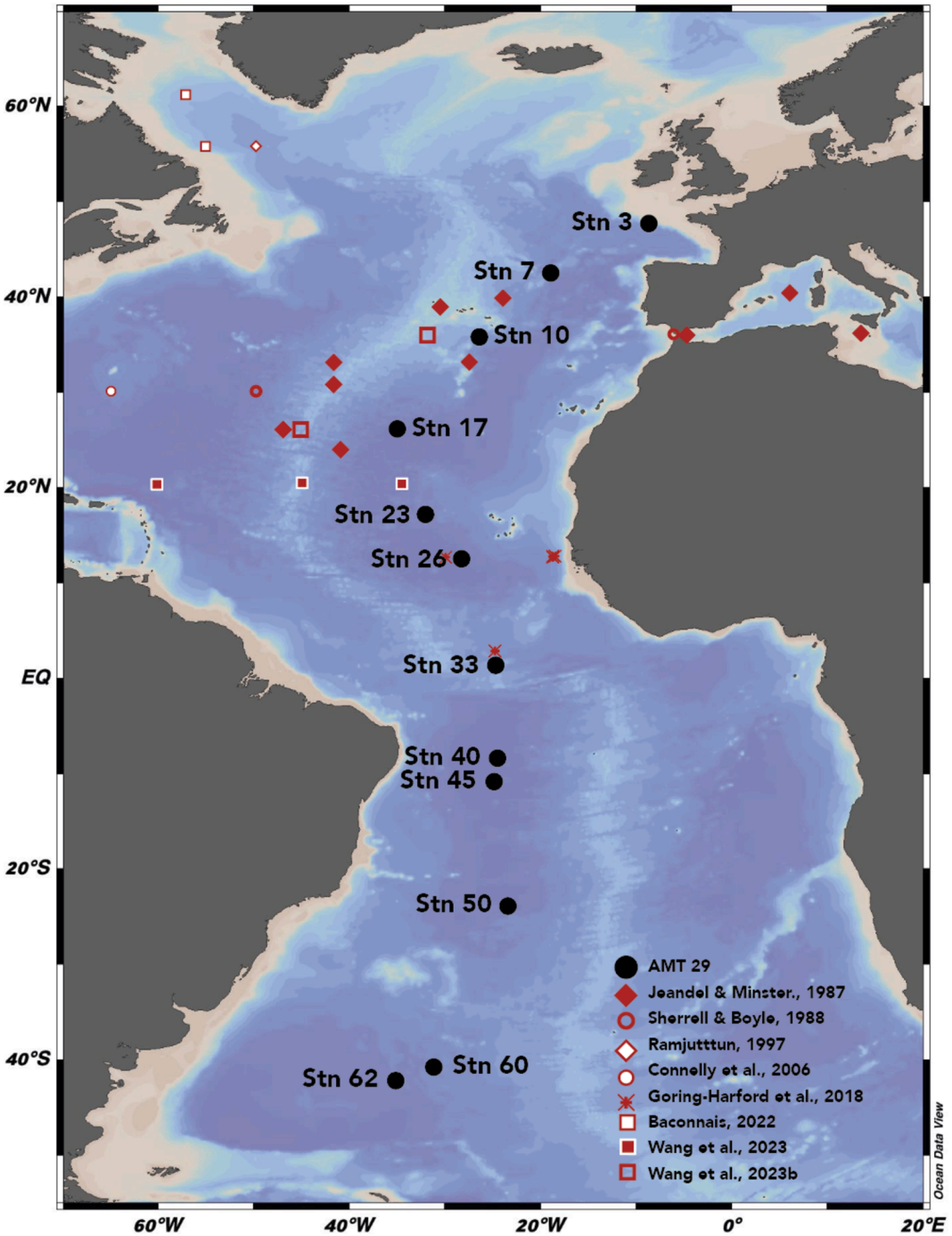

Fig. 1. Map of the sampling sites generated with Ocean Data View (ODV) (Schlitzer, 2022). Black dots represent the AMT 29 sampling site. Red and red-white symbols indicate the locations of previous Cr investigations in the Atlantic Ocean and Mediterranean (Jeandel and Minster, 1987; Sherrell and Boyle, 1988; Ramjuttun, 1997; Connelly et al., 2006; Goring-Harford et al., 2018; Baconnais 2022; Wang et al., 2023a).

Janssen et al., 2021; Bruggmann et al., 2023; Steiner et al., 2023). Hydrothermal sources may potentially impact the marine Cr budget, but their contribution to the global ocean inventory remains unclear. While the Kermadec ridge may act as a limited source of Cr (Janssen et al., 2023), the Rainbow and TAG vent sites act as a sink (Wang et al., 2023b). Finally, atmospheric deposition can lead to the supply of Cr to the surface ocean locally (Bonnand et al., 2013; Goring-Harford et al., 2018). However, the impact of atmospheric deposition on the overall marine Cr inventory is believed to be minimal (e.g., Schoenberg et al., 2008; Holmden et al., 2016; Goring-Harford et al., 2018; Pöppelmeier et al., 2021; Janssen et al., 2023; Wang et al., 2023a).

In the modern ocean, Cr can be found in two oxidation states: hexavalent Cr(VI), primarily as the CrO_4^{-2} species, and trivalent Cr(III), typically as $Cr(OH)_3$. Under oxic conditions, and at circum-neutral pH, Cr(VI) is thermodynamically stable and soluble in seawater (Elderfield, 1970). In contrast, Cr(III) is poorly soluble and thermodynamically unstable (Cranston, 1983; Achterberg and Van Den Berg, 1997), and readily adsorbs onto sinking mineral surfaces and particulate organic matter (Murray et al., 1983; Rue et al., 1997). Despite its thermodynamic instability, Cr(III) may account for up to ~15 % of the Cr species present in oxic waters with maximum concentrations at the ocean surface (e.g., Murray et al., 1983; Jeandel and Minster, 1987; Achterberg and Van Den Berg, 1997; Janssen et al., 2020). Chromium(III) may dominate locally under oxygen-depleted conditions such as those prevailing in oxygen minimum zones (OMZs) (e.g., Murray et al., 1983; Huang et al., 2021). Redox transformations result in stable isotope fractionation, with both oxidation and reduction reactions leading the reduced Cr(III) pool to become preferentially enriched in Cr light isotopes (e.g., Zink et al., 2010; Wanner and Sonnenthal, 2013; Milletto et al., 2021).

Previous sampling sites in the Atlantic Ocean from earlier studies are shown in (Fig. 1). These studies report [Cr] values ranging from 1.84 nmol kg^{-1} (Wang et al., 2023a) to 4.9 ± 0.3 nmol kg^{-1} (Jeandel and Minster, 1987), and $\delta^{53}Cr$ values ranging from +0.74 ± 0.03 ‰ (2SEM) (Baconnais, 2022) to +1.71 ± 0.11 ‰ (2SEM) (Goring-Harford et al., 2018). This is slightly lower [Cr] compared to the Pacific Ocean, which reflects the younger age of deep waters in the Atlantic Ocean, and consequently less accumulation of Cr in deep waters during lateral advection, as indicated by prior studies (Jeandel and Minster, 1987; Janssen et al., 2021; Pöppelmeier et al., 2021; Wang et al., 2023a). Concentrations of Cr within the Atlantic Ocean are slightly lower in surface waters than deep waters, accompanied by a relative enrichment of $\delta^{53}Cr$ compared to deeper waters (Jeandel and Minster, 1987; Goring-Harford et al., 2018; Wang et al., 2023a). Chromium concentration minima typically arise between 100 and 700 m, consistent with the scavenging of Cr(III) by sinking particles (Jeandel and Minster, 1987, Wang et al., 2023a) and associated with colloidal Fe-(oxyhydr)oxides (Wang et al., 2023a). Accumulation of [Cr] has been reported below 2000 m (Goring-Harford et al., 2018; Wang et al., 2023a, b). This may be, in part, due to benthic fluxes (e.g. Pöppelmeier et al., 2021; Wang et al., 2023a), with higher local fluxes near hydrothermal vents along the mid-Atlantic Ridge (Wang et al., 2023b). The low productivity of oligotrophic Atlantic waters and insufficient oxygen depletion suggest that biological export and removal in oxygen-depleted waters are unlikely to appreciably influence Cr distributions (Goring-Harford et al., 2018; Wang et al., 2023a).

Despite recent advances in our understanding of the marine Cr cycling, the Atlantic Ocean remains relatively understudied. To address this, we measured samples collected along the Atlantic Meridional Transect (AMT 29) ranging 50 °N to 40 °S, with the aim to enhance knowledge on the cycling of Cr on large oceanic scale. Our study investigated the impacts of water mass mixing, oxygen concentrations ($[O_2]$), and biological processes on the spatial and vertical Cr distribution, focusing on the upper 2000 m of the water column. By measuring [Cr] and $\delta^{53}Cr$ along the transect, our findings contribute to a deeper understanding of Cr dynamics in the modern ocean and improve the application of Cr isotopes as a paleoproxy.

2. Methods

2.1. Cr sampling

Seawater samples were collected between 13 October to 25 November 2019 along AMT 29 (Dall'Olmo, 2020) between Southampton (UK) and Punta Arenas (Chile) (Fig. 1) aboard RRS Discovery. Samples were collected using 20 L OTE Niskin bottles mounted on a stainless steel frame rosette. Samples for dissolved [Cr] and $\delta^{53}Cr$ (1 L) were collected by filtering seawater through pre-cleaned 0.2 μm ACROPAK® cartridge filters and were later acidified with ultra-pure HCl to reach a pH of ~1.7. The sampling LDPE bottles were pre-cleaned by soaking in an alkaline detergent (Citranox) bath for at least 3 days, rinsed with Milli-Q water, and filled with ultra-pure HCl 10 % for at least 1 week. Then, the sampling bottles were abundantly rinsed with Milli-Q water, closed, and double zip bagged until use.

2.2. Chromium purification chemistry

All the chemicals used during the procedure were suitable for trace metal clean use – HCl and HNO_3 were sub-boiling distilled with Teflon stills, ammonia and hydrogen peroxide solution were UpA grade (Romil), and ammonium peroxodisulfate was >99.0 % purity (TCI chemicals). A total of 68 ~1 L samples, collected at 12 stations ranging from the surface down to 2030 m depth, were processed for $\delta^{53}Cr$ analysis following (Rickli et al., 2019) (see also Moos and Boyle, 2019). Approximate [Cr] were first determined on ~30 mL aliquots by isotope dilution. First the aliquots were spiked with 200 μL of 5 ppb ^{50}Cr, to determine [Cr] for spiking purposes. Chromium from the aliquots was purified with Mg co-precipitation by adding ~0.7 to 1 mL NH_3, then the aliquots were centrifuged, and the remaining precipitate dissolved in 2 mL 1 M HNO_3. Then, chromatographic cation exchange columns (AG50W-X8) were used to separate Cr from the matrix (Yamakawa et al., 2009). To determine $\delta^{53}Cr$ and final [Cr], a double spike ($^{50-54}Cr$) approach was used. After spiking, the samples were left for at least 48 h to equilibrate, then co-precipitated (as explained above yet with ~7 mL NH_3 per L) and left overnight for the precipitate to settle (Moos and Boyle, 2019; Rickli et al., 2019). The precipitate was extracted by centrifugation, dissolved in 2 M HCl and transferred to clean Teflon vials and dried. The dried sample was taken up in 9 mL 0.022 M HCl and processed for column chromatography. Column chromatography followed a two-step procedure starting with anion exchange using AG1-X8 resin (Rickli et al., 2019; Ball and Bassett, 2000; Janssen et al., 2020; Nasemann et al., 2020), and cation exchange using AG 50W-X8 resin (Yamakawa et al., 2009; Rickli et al., 2019). After column chromatography, the samples were collected in clean Teflon vials, dried and dissolved in 1 mL 0.5 M HNO_3. Procedural blanks were processed along each set of samples, with an average Cr of 1.09 ng, of which the ammonium peroxodisulfate oxidizing agent is the primary source (see Rickli et al., 2019).

The stable isotopic composition of Cr and [Cr] were analyzed on a Neptune Plus MC-ICP-MS (Rickli et al., 2019). Results of $\delta^{53}Cr$ are reported relative to NIST SRM 979. OSIL waters were used as an external reproducibility and follow the chemistry described above. The uncertainty from OSIL measurements on the $\delta^{53}Cr$ is ±0.06 ‰ (2SD) and ±0.24 nmol kg^{-1} for [Cr] based on 6 full replicates of ~0.5 L samples measured at the universities of Bern (UniBe) and Lausanne (UNIL) (Table S1).

Most of the samples presented here were processed and measured at the Institute of Geology Sciences at UniBe and a smaller portion of the sample set was analyzed at the Institute of Earth Sciences at UNIL (Table 1). The resins (AG 50W-X8 and AG1-X8), columns, Cr spikes and Neptune methods were the same for both laboratories. Replicates conducted to ensure the reliability of the data processed at UNIL generally

Table 1
Hydrographic, macronutrients, and Cr results originate from AMT 29 cruise (Dall'Olmo et al., 2020).

Station	Depth [m]	Latitude °N	Longitude °E	Temperature [°C]	Salinity PSU	Oxygen [μmol l^{-1}]	Chlorophyll [μg l^{-1}]	Nitrate [μmol l^{-1}]	Phosphate [μmol l^{-1}]	Silicate [μmol l^{-1}]	δ^{53}Cr (‰)	2 SEM (‰)	[Cr] nmol kg^{-1}	Labo
3	17	47.14	−9.2	16.2	35.56	231.94	0.47	0.55	0.07	1.06	1.14	0.03	2.85	Bern
3	103	47.14	−9.2	12.5	35.60	231.43	0.031	9.37	0.45	3.39	1.09	0.03	3.04	Bern
3	304	47.14	−9.2	11.4	35.52	226.82	0.01	11.91	0.58	4.54	1.08	0.03	2.78	Bern
3	508	47.14	−9.2	10.8	35.48	209.54	0.00	13.34	0.62	5.73	1.05	0.03	2.78	Bern
7	13	42.14	−19.12	19.6	36.17	220.68	0.07	0.03	0.02	0.95	1.12	0.04	2.72	Bern
7	103	42.14	−19.12	15.6	36.08	216.66	0.13	4.69	0.21	1.99	1.09	0.04	2.68	Bern
7	304	42.14	−19.12	13.4	35.74	214.63	0.01	10.76	0.55	3.72	1.07	0.04	2.83	Bern
7	508	42.14	−19.12	11.9	35.56	213.33	0.01	11.48	0.60	4.66	1.13	0.03	2.92	Bern
10	5	35.55	−26.53	22.9	36.50	210.46	0.03	0.04	0.02	1.43	1.12	0.03	2.96	Bern
10	38	35.55	−26.53	22.7	36.50	211.48	0.04	0.04	0.02	1.14	1.20	0.02	2.91	Lausanne
10	53	35.55	−26.53	19.3	36.23	241.83	0.10	0.09	0.02	1.70	1.12	0.04	2.93	Bern
10	133	35.55	−26.53	15.7	36.11	211.04	0.05	4.34	0.20	2.62	1.13	0.05	2.86	Bern
10	305	35.55	−26.53	13.3	35.76	196.69	0.01	11.04	0.52	3.89	1.11	0.03	2.74	Lausanne
10	507	35.55	−26.53	11.8	35.59	190.09	0.00	14.21	0.74	5.69	1.02	0.04	2.51	Bern
17	59	26.08	−35.11	26.0	37.56	199.81	0.02	0.02	0.02	0.99	1.11	0.04	2.98	Bern
17	173	26.08	−35.11	20.0	36.86	195.23	0.02	0.82	0.04	1.30	1.08	0.05	2.91	Bern
17	304	26.08	−35.11	17.2	36.39	184.61	0.00	6.21	0.29	2.28	0.98	0.05	2.54	Bern
17	506	26.08	−35.11	13.6	35.82	177.64	0.00	12.24	0.68	5.05	0.95	0.06	2.59	Bern
23	8	17.17	–32.09	27.4	36.77	194.92	0.02	0.02	0.02	1.23	1.14	0.03	2.99	Bern
23	42	17.17	–32.09	27.1	36.78	196.83	0.08	0.04	0.02	0.96	1.11	0.02	2.99	Bern
23	202	17.17	–32.09	15.4	36.01	104.55	0.05	19.38	0.92	6.23	1.02	0.04	2.75	Bern
23	404	17.17	–32.09	11.8	35.50	83.12	0.03	27.58	1.38	11.17	1.05	0.03	2.82	Bern
23	860	17.17	–32.09	6.7	34.91	114.43	0.02	33.67	1.87	23.73	1.00	0.04	3.16	Bern
23	1012	17.17	–32.09	6.1	34.93	134.47	0.02	32.8	1.9	25.21	1.00	0.04	3.04	Bern
23	1518	17.17	–32.09	4.5	35.01	201.30	0.01	24.75	1.39	22.80	0.93	0.05	2.91	Bern
23	2030	17.17	–32.09	3.6	34.98	229.34	0.02	22.32	1.26	25.25	0.95	0.04	2.88	Bern
26	5	12.44	−28.3	28.3	35.98	191.82	0.07	0.05	0.02	1.84	0.98	0.03	3.24	Bern
26	43	12.44	−28.3	19.1	35.80	118.10	0.81	8.01	0.56	2.87	1.06	0.03	2.93	Bern
26	103	12.44	−28.3	13.6	35.41	72.16	0.05	24.86	1.46	9.35	1.08	0.02	3.27	Lausanne
26	204	12.44	−28.3	12.1	35.27	68.11	0.04	24.04	2.01	10.39	1.05	0.03	3.20	Bern
26	508	12.44	−28.3	9.4	35.09	48.16	0.04	33.77	2.01	16.20	0.91	0.03	3.23	Bern
33	34	1.4	−25	28.3	35.41	193.28	0.08				1.05	0.03	3.00	Bern
33	152	1.4	−25	14.0	35.43	111.61	0.03	21.11	1.17	8.11	1.09	0.04	2.74	Bern
33	810	1.4	−25	4.9	34.55	144.36	0.02	34.99	2.06	31.21	1.07	0.04	2.90	Bern
33	1519	1.4	−25	4.4	34.96	215.22	0.02	23.37	1.32	20.08	1.07	0.03	2.95	Bern
33	2030	1.4	−25	3.5	34.96	239.10	0.03	20.68	1.21	22.01	0.98	0.03	2.87	Bern
40	46	−8.24	−24.59	25.7	36.35	199.27	0.06	0.02	0.07	1.09	1.06	0.03	3.08	Bern
40	304	−8.24	−24.59	9.4	34.86	86.10	0.03	30.16	1.84	13.34	0.96	0.03	3.01	Bern
40	507	−8.24	−24.59	6.9	34.60	104.99	0.04	34.10	2.08	19.98	0.94	0.03	3.09	Bern
40	811	−8.24	−24.59	4.7	34.47	148.61	0.03	33.52	2.16	31.27	0.95	0.03	3.25	Bern
40	1266	−8.24	−24.59	4.3	34.81	183.78	0.01	33.66	2.18	34.52	0.99	0.03	3.32	Bern
40	1519	−8.24	−24.59	4.1	34.94	217.58	0.03	23.23	1.44	20.75	0.99	0.04	2.88	Bern
40	2031	−8.24	−24.59	3.4	34.95	235.49	0.01	21.17	1.34	24.63	1.03	0.04	3.03	Bern
45	32	−15.26	−25	25.2	37.09	201.46	0.02				1.02	0.03	3.13	Lausanne
45	57	−15.26	−25	24.7	37.06	204.44	0.04	0.02	0.08	0.92	1.10	0.03	3.17	Bern
45	162	−15.26	−25	22.8	36.86	201.50	0.22	0.07	0.16	0.92	1.05	0.04	3.11	Bern
45	405	−15.26	−25	9.6	34.80	134.65	0.03	26.60	1.67	12.56	0.99	0.03	3.17	Bern
45	710	−15.26	−25	4.7	34.42	171.45	0.01	33.46	2.15	30.28	0.97	0.03	3.17	Bern
45	1519	−15.26	−25	4.0	34.89	207.21	0.01	25.03	1.58	25.12	1.00	0.03	3.01	Bern
45	2031	−15.26	−25	3.2	34.91	228.95	0.02	22.78	1.47	31.95	0.94	0.04	3.11	Bern
50	4	–23.43	−24.55	23.5	36.91	206.12	0.02	0.02	0.10	1.34	1.09	0.04	3.15	Bern
50	213	–23.43	−24.55	18.5	36.02	199.51	0.06	1.96	0.29	1.72	0.96	0.03	2.97	Bern
50	304	–23.43	−24.55	14.6	35.38	195.83	0.01	7.50	0.56	3.13	1.02	0.04	3.03	Bern

(*continued on next page*)

Table 1 (*continued*)

Station	Depth [m]	Latitude °N	Longitude °E	Temperature [°C]	Salinity PSU	Oxygen [µmol l^{-1}]	Chlorophyll [µg l^{-1}]	Nitrate [µmol l^{-1}]	Phosphate [µmol l^{-1}]	Silicate [µmol l^{-1}]	δ^{53}Cr (‰)	2 SEM (‰)	[Cr] nmol kg^{-1}	Labo
50	508	−23.43	−24.55	10.8	34.89	183.64	0.00	17.63	1.17	7.34	0.97	0.03	3.03	Bern
60	26	−40.21	−31.2	13.2	35.07	261.45	0.86	4.39	0.43	2.58	0.96	0.04	3.01	Bern
60	202	−40.21	−31.2	9.1	34.62	236.41	0.03	16.28	1.05	6.19	0.98	0.04	3.06	Bern
60	405	−40.21	−31.2	5.3	34.22	246.37	0.03	26.15	1.61	12.96	0.92	0.03	3.22	Bern
60	609	−40.21	−31.2	4.1	34.17	250.58	0.02	28.69	1.79	19.81	1.01	0.02	3.09	Bern
60	1013	−40.21	−31.2	3.1	34.33	196.86	0.02	33.82	2.12	44.04	0.89	0.03	3.40	Bern
62	5	−41.54	−35.26	11.4	34.49	278.68	1.35	6.69	0.48	0.54	1.09	0.06	3.18	Lausanne
62	18	−41.54	−35.26	11.3	34.48	280.00	1.75	6.88	0.53	0.14	0.99	0.03	3.07	Bern
62	103	−41.54	−35.26	8.4	34.53	249.15	0.03	16.83	1.04	5.32	0.99	0.06	2.98	Lausanne
62	255	−41.54	−35.26	7.1	34.42	245.19	0.01	18.59	1.22	6.85	0.97	0.04	3.02	Bern
62	407	−41.54	−35.26	4.9	34.20	250.21	0.02	26.70	1.59	12.93	0.96	0.03	2.92	Bern
62	611	−41.54	−35.26	3.8	34.18	243.13	0.02	29.60	1.77	22.02	0.89	0.03	2.92	Bern
62	1013	−41.54	−35.26	3.0	34.38	187.06	0.02	34.50	2.10	50.44	0.90	0.04	3.57	Bern
62	1778	−41.54	−35.26	2.9	34.75	185.43	0.02	34.64	2.08	60.44	0.86	0.04	3.96	Bern
62	2034	−41.54	−35.26	2.7	34.79	192.55	0.02	28.92	1.76	59.92	0.87	0.03	3.30	Bern

agreed with data processed at UniBe (Table S2).

3. Study area and hydrography

The AMT program, launched in 1995, surveys a range of biogeochemical parameters along a meridional transect across the Atlantic basin between the UK and South America. The AMT 29 transect encompasses 6 major water masses including North Atlantic Central Water (NACW), South Atlantic Central Water (SACW), Mediterranean Water (MW), Antarctic Intermediate Water (AAIW), Upper Circumpolar Deep Water (UCDW) North Atlantic Deep Water (NADW) (Fig. 2). Typically found at depths between 200 and 500 m, SACW has a temperature range of 10 to 26 °C and a salinity ranging between 35.0 and 37.3 (Stramma and England, 1999; Tomczak and Godfrey, 2003; Bianchi et al., 1993; Blanke et al., 2006). In the northern part of the transect, NACW exhibits similar characteristics to SACW, with a temperature range of 8.0 to 18 °C, salinity between 35.2 and 36.7, and generally low nutrient content (Liu and Tanhua, 2021). The most saline water mass of the transect is MW, with a temperature range of 2.6–11 °C (Emery, 2003). Composing most of the deep water mass along our transect, NADW is formed in the high northern latitudes and flows southward at depths greater than 1500 m, below AAIW (Emery, 2003). NADW is relatively saline, oxygenated, and nutrient-depleted compared to AAIW, with a temperature range of 1.5–4 °C and salinity between 34.8 and 35.0 (Emery, 2003). In the southernmost station, AAIW flows northward around 800 m, distinguishable by its low salinity relative to NADW and temperature around 4 °C (Talley, 2011). This northward-flowing water mass transports nutrient-rich subsurface waters into the Atlantic basin. In the South Atlantic, UCDW appears below AAIW with a potential temperature around 3 °C and salinity between 34.8 and 34.9 (Talley, 2011).

4. Results

4.1. Dissolved Cr concentration

Dissolved [Cr] values ranged between 2.51 and 3.96 nmol kg^{-1} (n = 68) with a majority of the data clustering within a narrower range of 2.75–3.39 nmol kg^{-1} (n = 56) (Fig. 3), (Table 1). There are only slight vertical variations in [Cr] within individual depth profiles, typically <0.5 nmol kg^{-1}, except for the southernmost station (station 62), for which concentrations significantly increase at depth. The northernmost part of the transect corresponds to the lowest [Cr], with values gently increasing (<0.75 Cr nmol kg^{-1}) southwards, beyond station 23. There is no significant change in [Cr] in dysoxic environments (grey shading in Fig. 3).

4.2. Dissolved chromium isotope compositions

δ^{53}Cr values ranged between +0.86 ± 0.04 ‰ (2SEM) to +1.20 ± 0.02 ‰ (2SEM). Generally, δ^{53}Cr shows little variation along depth at each station. Greater variations are observed for stations 10, 23, and 26, at which depth-dependent δ^{53}Cr gradients are slightly more pronounced. Between stations, trends are rather unpredictable. For instance, in the upper 500 m at stations 17 and 23, δ^{53}Cr decreases with depth while at stations 3 and 7, the variation of δ^{53}Cr remains within uncertainty. Below 500 m, stations are characterized by the lowest δ^{53}Cr values, except for station 40. The northernmost part of the transect corresponds to higher δ^{53}Cr, and δ^{53}Cr decreases southward (Fig. 3). Much like [Cr], dysoxic environments do not appear to significantly affect the δ^{53}Cr profiles (Fig. 3).

4.3. Relationship between ln([Cr]) and δ^{53}Cr

A general Rayleigh-type fractionation between ln(Cr) and δ^{53}Cr throughout the ocean was first proposed by Scheiderich et al., (2015), based on the strong correlation between δ^{53}Cr and ln(Cr) globally. The

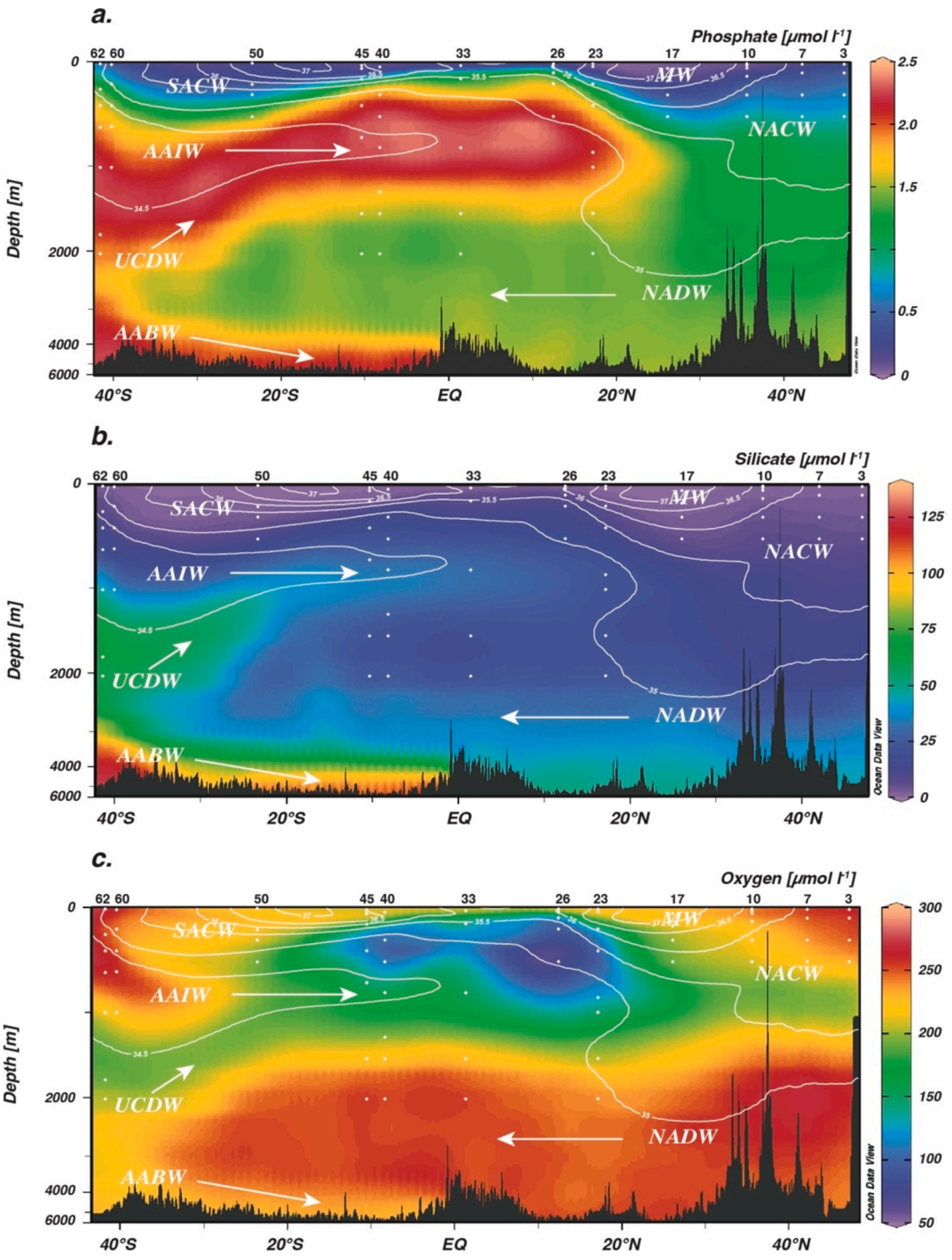

Fig. 2. AMT 29 section with WOA 2018 (Garcia et al., 2019) data set for a. phosphate (PO_4), b. silicate (Si), c. oxygen (O_2). Each panel comprises salinity (white lines) and water masses with their flowing direction (white arrows). AMT 29 Cr sampling sites are represented by white dots and black numbers above indicate the station numbers. South Atlantic Central Water (SACW), Antarctic Intermediate Water (AAIW), Upper Circumpolar Deep Water (UCDW), Antarctic Bottom Water (AABW), Mediterranean Water (MW), North Atlantic Central Water (NACW), North Atlantic Deep Water (NADW).

central mechanistic control that has been suggested relates to the reduction of Cr(VI) to Cr(III), followed by its adsorption onto particles (scavenging) and removal from seawater, associated primarily with biological productivity in shallow waters and oxygen-depleted zones (OMZs). This reduction leads to lower [Cr] and enriched δ^{53}Cr, while deeper remineralization of sinking particles results in higher [Cr] and lower δ^{53}Cr (Scheiderich et al., 2015; Janssen et al., 2020, 2021; Moos et al., 2020; Nasemann et al., 2020; Huang et al., 2021). The latest compilation of open ocean Cr data, excluding AMT 29 data, exhibits an R^2 of 0.70 and a slope of -0.66 ± 0.02 ‰ (n = 500; Scheiderich et al., 2015; Moos, 2018; Goring-Harford et al., 2018; Moos and Boyle, 2019; Rickli et al., 2019; Nasemann et al., 2020; Janssen et al., 2020, 2021, 2023; Huang et al., 2021; Baconnais, 2022; Wang et al., 2023a,b) (Fig. 4).

Our AMT 29 data deviate from the global compilation, exhibiting a narrow range of [Cr], while δ^{53}Cr exhibits a more heterogenous range (Fig. 4). The correlation between δ^{53}Cr and ln(Cr) in the AMT 29 data is weaker, with an R^2 of only 0.17 and a slope of -0.42 ± 0.12 ‰ (n = 68). This divergence suggests that the application of the Rayleigh-type fractionation model may not be appropriate for the Atlantic Ocean.

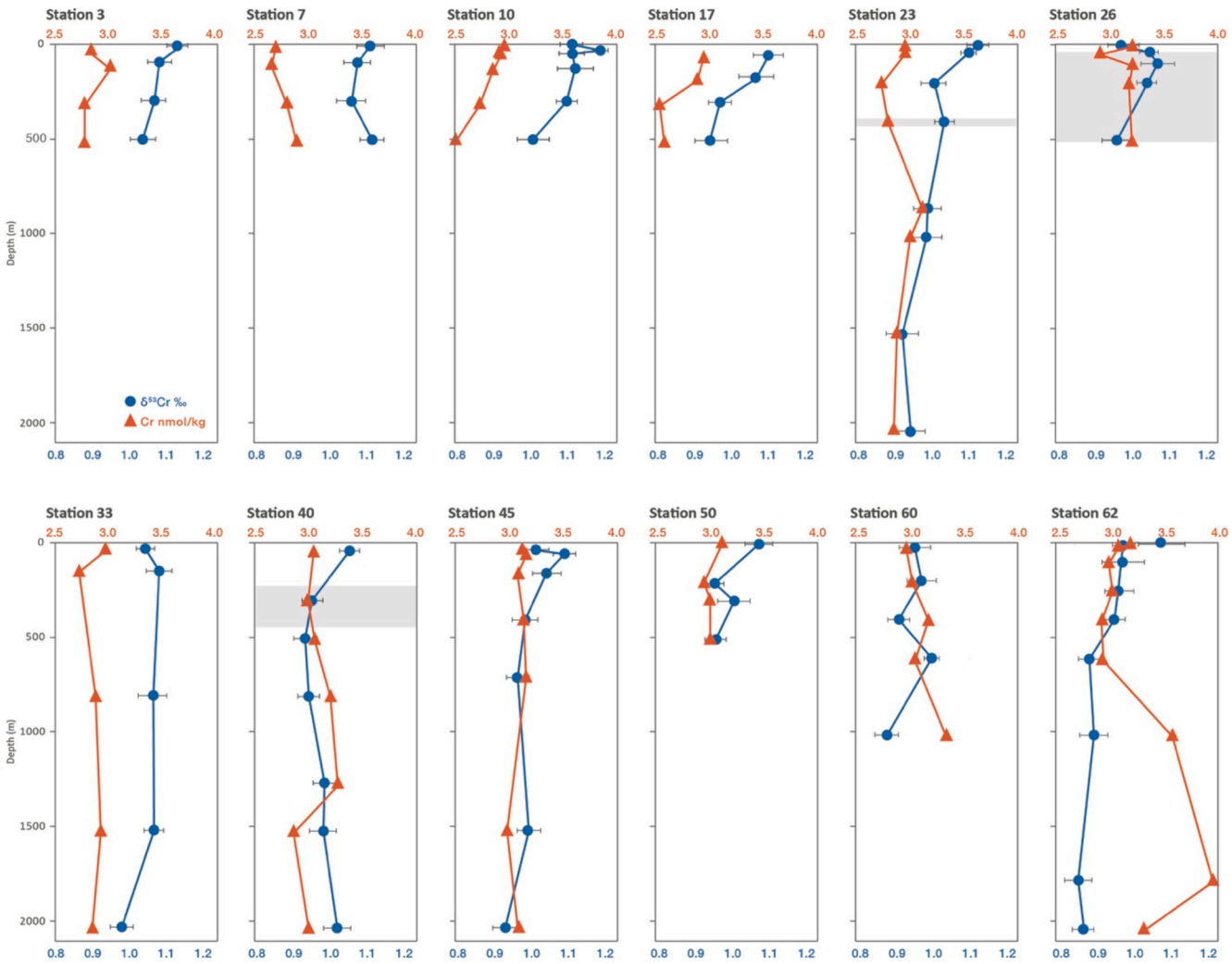

Fig. 3. Depth profiles of $\delta^{53}Cr$ in blue and [Cr] in orange. Grey shadings indicate dysoxic (9.2–92 O_2 μmol kg^{-1} (Tyson and Pearson 1991)) environments.

Mechanisms explaining deviation from the global array are outlined in section 5 below.

4.4. *Comparison with existing Atlantic data*

Our data agree well with previous studies focusing on documenting the cycling of Cr in the Atlantic Ocean, with similar ranges of [Cr]. Indeed, [Cr] in our study range from 2.51 to 3.96 nmol kg^{-1}, consistent with findings previously reported by Jeandel and Minster (1987), Sherrell and Boyle (1988), Ramjuttun (1997), and Baconnais (2022) (Figure S1). Depth profiles are characterized by rather stable values in the upper 2000 m, as observed previously (Jeandel & Minster, 1987; Ramjuttun, 1997) and in contrast to distributions in the other major ocean basins (e.g. Scheiderich et al., 2015; Rickli et al., 2019; Moos & Boyle, 2019; Janssen et al., 2020). Finally, fine-scale [Cr] minima within the 100–700 m depth are reported at multiple stations (23, 45, and 60), consistent with previous findings (Jeandel and Minster, 1987; Wang et al., 2023a).

However, despite this broad agreement, some discrepancies are apparent between our data and recent studies from the (sub)tropical Atlantic (Goring-Harford et al., 2018; Wang et al., 2023a). When adjacent stations are compared (AMT29 stations 26 and 33 with stations 18 and 11.5 in Goring-Harford et al., 2018; AMT29 station 23 compared with station 6 in Wang et al., 2023a), both our [Cr] and $\delta^{53}Cr$ values are offset from the literature values (+0.05 to +1.04 nmol kg^{-1} and 0.05–0.38 ‰, respectively). The underlying reasons for this remain unclear, and may reflect differences in sample processing and/or analytical protocols. Our results, based on $Mg(OH)_2$ co-precipitation, a method used in multiple previous studies (Moos, 2018; Moos and Boyle, 2019; Rickli et al., 2019; Davidson et al., 2020; Nasemann et al., 2020; Janssen et al., 2020, 2021, 2023; Huang et al., 2021), provides robust and reproducible results amongst different labs (Table 1 and Table S1, S2). Our spike calibration and laboratory procedures were validated repeatedly by accurate determination of [Cr] and $\delta^{53}Cr$ in certified reference materials (Janssen et al., 2022. Additionally, previous data using our Cr double spike and method show oceanographic consistency between different studies along the same water masses (e.g., Moos and Boyle, 2019; Janssen et al., 2020, 2021, 2023). Our [Cr] data compare well with the majority of Atlantic Cr data from the past four decades (Figure S1; Jeandel and Minster, 1987; Sherrell and Boyle, 1988; Ramjuttun, 1997; Baconnais, 2022), and our data from NADW throughout our transect are consistent with literature endmember values (section 5.1; Ramjuttun, 1997; Baconnais, 2022). In contrast, a recent study that reported Cr data from the subtropical Atlantic identified lower [Cr] in intercalibration material (Wang et al., 2023a). These observations suggest that some recent Atlantic Cr data may be slightly offset in their [Cr] and $\delta^{53}Cr$ values.

Consequently, it becomes evident that there is a need to establish a robust seawater standard for comparative analysis of data obtained through diverse methodologies. So far, the current standard used to

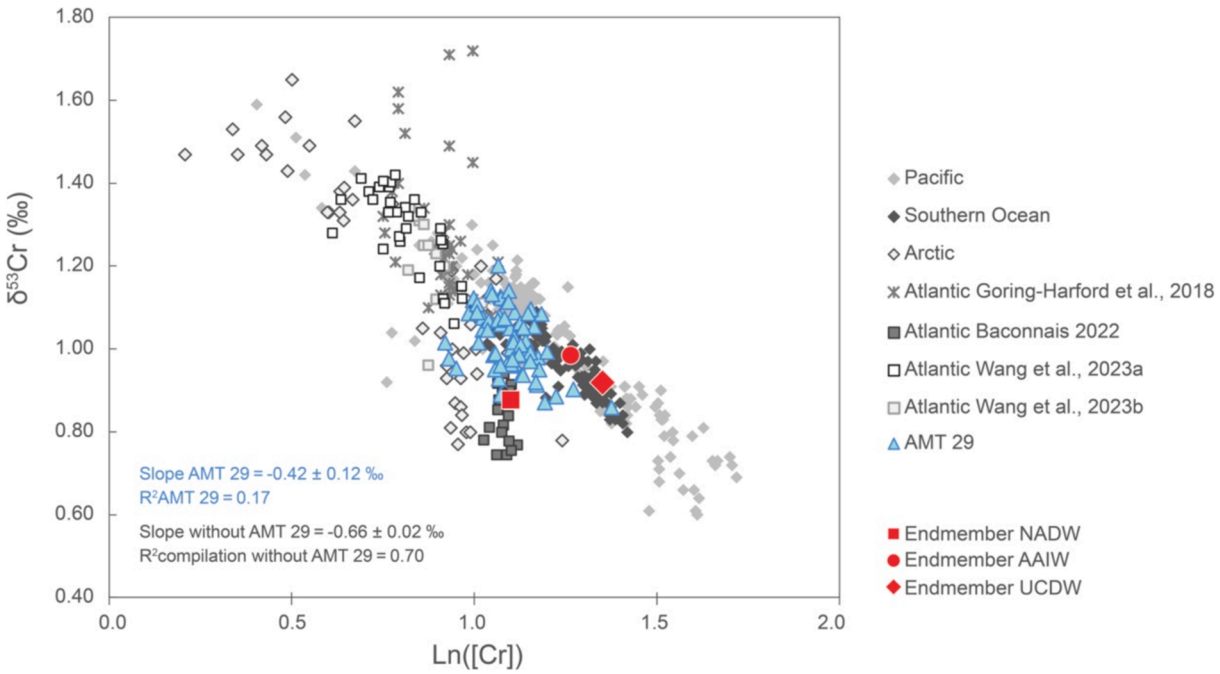

Fig. 4. Linear relationship between δ^{53}Cr and [Cr] from previous studies (grey symbols) and AMT 29 (blue triangles). Pacific data have previously been published by Scheiderich et al. (2015); Moos and Boyle (2019); Nasemann et al. (2020); Janssen et al. (2020, 2021, 2023); Moos et al. (2020); Huang et al. (2021), Southern Ocean data by Rickli et al. (2019), Arctic data by Scheiderich et al. (2015) and Moos, (2018), Atlantic data (excluding data impacted by hydrothermal fluids) by Goring-Harford et al. (2018) and Wang et al. (2023a, b), and Labrador Sea by Baconnais (2022). Red symbols indicate Cr endmembers: NADW values are defined using data from (Baconnais, 2022), while AAIW and UCDW values are based on (Janssen et al., 2021).

assess external reproducibility is OSIL; however, its sampling conditions may lead to variable, inhomogeneous levels of Cr (Scheiderich et al., 2015; Rickli et al., 2019; Nasemann et al., 2020; Baconnais, 2022; Wang et al., 2023a; this study). A dedicated seawater standard for Cr, designed for trace metal studies and devoid of batch-to-batch variability, should be adopted to ensure a more unified and reliable framework for interpreting Cr data.

5. Discussion

The distribution and cycling of Cr in the water column can be influenced by a variety of processes, all of which have the potential to induce shifts in δ^{53}Cr (e.g., Fig. 7 in Janssen et al., 2021). We examine the contribution of several key processes on the biogeochemical cycling of Cr in the Atlantic Ocean in the section below. These processes include water mass mixing, Cr removal in OMZs, and Cr transfer to depth by the biological carbon pump.

5.1. *Water mass mixing and horizontal advection*

In the Atlantic Ocean, lateral advection and water mass mixing were demonstrated to play an important role in modulating the distribution of major nutrients (e.g., Sarmiento et al., 2007) and dissolved trace metals such as Cd, Ni, and Zn (e.g., Saager et al., 1997; Wu et al., 2014; Bruland et al., 2014; Conway and John 2015; Middag et al., 2019; Chen et al., 2024), and may thus also impact the cycling of Cr. Indeed, advection and mixing have been reported as major controls on the distribution of Cr in the upper 1000 m of the Southern Ocean (Rickli et al., 2019). To assess the role of water mass mixing in the Atlantic, one must first consider the relevant water masses and their biogeochemical characteristics. Based on deep water circulation in the Atlantic and the depth range of our stations, AAIW, NADW and UCDW are the intermediate and deep water masses, respectively, that set expectations for mixing-based controls on [Cr] and δ^{53}Cr.

In the northern section of our transect, NADW flows southward around 1500–2500 m (Fig. 5), and is characterized by [Cr] ~2.89 nmol kg^{-1} and δ^{53}Cr ~+0.94 ± 0.04 ‰ (2SEM) (station 23, 17.17 °N). The NADW endmember in the Labrador Sea has [Cr] of approximately 2.97 nmol kg^{-1} and δ^{53}Cr +0.89 ± 0.04 ‰ (2SEM) (Baconnais, 2022). Comparing the NADW Cr endmember with our measurements, our values for NADW at 17 °N are within analytical uncertainty of previous data from the Labrador Sea. During its southward advection, the macronutrient inventory of NADW slightly increases, while the apparent oxygen utilization (AOU) doubles, yet Cr compositions remain stable with a slight accumulation during advection (2.87–3.30 nmol kg^{-1} and most of the δ^{53}Cr values overlap within uncertainty) (Fig. 6, Figure S2). This constancy in Cr compositions, despite coherent changes in other biogeochemical parameters, is consistent with lateral advection primarily controlling the distribution of Cr, and with basin scale distributions reflecting the transport of a relatively unmodified NADW endmember signal.

At the southernmost station (station 62, 41.5 °S), AAIW (Fig. 5) is characterized by [Cr] ~2.92 nmol kg^{-1} and δ^{53}Cr ~+0.89 ± 0.03 ‰ (2SEM). The average endmember Cr composition of AAIW is ~3.6 nmol kg^{-1} and δ^{53}Cr +0.98 ± 0.03 ‰ (2SEM) at ~54 °S (Janssen et al., 2021). The endmember [Cr] for AAIW is higher than the [Cr] observed along AMT 29 (Figure S3). Similarly, the AAIW δ^{53}Cr endmember value is slightly higher than our δ^{53}Cr measurements. During the northward advection of AAIW, macronutrient concentrations and AOU both increase but remain within similar ranges (Fig. 6, Figure S3), consistent with water column organic matter remineralization. As such, the subsurface remineralized Cr pool may provide a source of isotopically light Cr to the surface ocean. However, we observe a decrease in [Cr] and a concomitant increase in δ^{53}Cr, which may be attributed to mixing with other water masses. Along AMT 29, AAIW likely mixes with NADW, which flows southward below AAIW (Figs. 5 and 6), and which has lower [Cr] and similar or slightly lower δ^{53}Cr than AAIW. In this region, MW and NACW may also contribute to the Cr composition, although their influence may be smaller than the predominant water masses AAIW and NADW. Therefore, during mixing it appears that the AAIW Cr

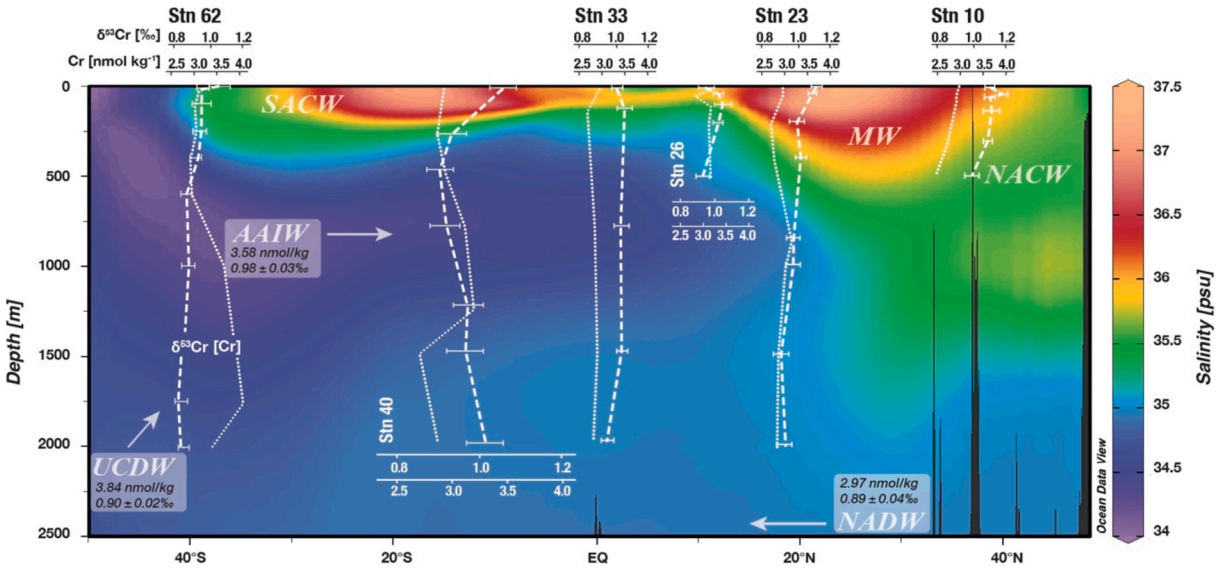

Fig. 5. AMT 29 section of salinity and overlapping $\delta^{53}Cr$ (dashed white line) and [Cr] (dotted white line) with water masses and the respective flow directions. Station 40 has a larger scale to better visualize the vertical Cr variations. Salinity data originate from WOA 2018. Water masses and their Cr endmember are in the white squares. Cr endmember for UCDW ([Cr] = 3.84 nmol kg^{-1}; $\delta^{53}Cr = +0.9 \pm 0.02$ ‰) and Cr endmember for AAIW ([Cr] = 3.58 nmol kg^{-1}; $\delta^{53}Cr = +0.98 \pm 0.03$ ‰) are defined after Janssen et al. (2021); Cr endmember for NADW ([Cr] = 2.97 nmol kg^{-1}; $\delta^{53}Cr = +0.89 \pm 0.04$ ‰) is defined after Baconnais, (2022).

inventory is diluted by more saline, Cr-depleted NADW (Fig. 5, Fig. 6). A similar interaction has been observed with AAIW and NADW mixing in the Southern Ocean (Rickli et al., 2019). The result of this mixture would be a decrease in [Cr] and similar or slightly lower $\delta^{53}Cr$. Therefore, the mixing of these different Cr pools in the Atlantic Ocean, despite varying [Cr] concentrations, results in largely invariant isotopic gradients along the meridional transect.

Below AAIW, at around 1000–2000 m, northward-flowing UCDW (Fig. 5) is characterized by [Cr] ranging from 3.57 to 3.96 nmol kg^{-1} and $\delta^{53}Cr$ ~+0.88 ± 0.04 ‰ (2SEM) (station 62, 41.54 °S). The UCDW endmember (~60 °S) has [Cr] ~3.84 nmol kg^{-1} and $\delta^{53}Cr$ ~+0.90 ± 0.02 ‰ (2SEM) (Janssen et al., 2021). Tracing UCDW-impacted waters along the AMT transect, [Cr] decrease along with decrease in [Si], while AOU remains constant as waters advect northward. Regarding $\delta^{53}Cr$ values, it remains constant (Fig. 6, Figure S2). The decrease in [Si] along largely invariant AOU may be explained by mixing with NADW (Fig. 5, Fig. 6, Figure S2), which also accounts for the observed decrease in [Cr]. At station 62–2034 m ([Cr] = 3.3 nmol kg^{-1}), [Cr] is lower, as is $[PO_4^{3-}]$, compared to UCDW, indicating a potential influence of lower circumpolar deep water (LCDW). Compared to the LCDW endmember ([Cr] ~3.89 nmol kg^{-1} and $\delta^{53}Cr$ ~+0.90 ± 0.02 ‰ (2SEM) (Janssen et al., 2021)), [Cr] decrease northward along with macronutrient concentrations. At station 62, at a depth of 1778 m, [Cr] is 3.96 nmol kg^{-1} within UCDW, while just below, at a depth of 2030 m, NADW has [Cr] of 3.30 nmol kg^{-1}. This significant difference in [Cr] between these depths highlights the influence of NADW on UCDW. As NADW mixes with UCDW further north, it dilutes [Cr] in UCDW, resulting in lower [Cr]. Despite this dilution, the $\delta^{53}Cr$ values remain unchanged.

Given the role of water mass mixing and advection on shaping macronutrient distributions in the Atlantic Ocean (e.g., Brzezinski and Jones, 2015), the importance of water mass advection may also be central in shaping Cr-macronutrient relationships. The highest [Cr] and [Si] are associated with UCDW ([Cr] = 3.57 to 3.96 nmol kg^{-1}), while NADW is characterized by relatively lower [Cr] (~3 nmol kg^{-1}) and lower [Si] (Fig. 6). AAIW falls between UCDW and NADW in Cr-Si space, and surface waters are generally characterized by lower [Si] compared to NADW, with [Cr] similar to or slightly lower than those in NADW and AAIW (Fig. 6). This behavior is inconsistent with in situ biogeochemical cycling, such as the coupled transfer of Cr and Si from surface waters to deeper layers by sinking particles. Rather, the tight Cr-Si correlation reflects the importance of advection for the transport of nutrients and nutrient-type elements. This pattern has been previously described for other metal-macronutrient pairs (Sunda and Huntsman, 2000; Sarmiento et al., 2004; Wyatt et al., 2014; Vance et al., 2017; Ellwood et al., 2018; Middag et al., 2019; George et al., 2019). Water mass regulation of Cr-Si trends is consistent with decreased regeneration of nutrient-type elements with deeper maxima in the Atlantic Ocean relative to other ocean basins (e.g., Sarmiento et al., 2007).

The complexity of Cr distribution and behavior in the Atlantic Ocean is further underscored by the weak linear relationship between $\delta^{53}Cr$ and ln([Cr]) observed in our study (Fig. 4). While the global compilation of oceanic data shows a stronger correlation consistent with Rayleigh-type fractionation, our AMT 29 data reveal a significantly weaker correlation (Fig. 4). This discrepancy suggests that a theoretical closed-system Rayleigh fractionation model, which primarily considers unidirectional removal or addition processes, and which does not accurately constrain mixing processes, may not adequately capture the dynamics of Cr in the Atlantic Ocean. Consequently, Cr-macronutrient trends in this part of the Atlantic Ocean should be interpreted to reflect advection and water mass mixing rather than primarily reflecting vertically-acting processes (i.e. biological uptake, export, and regeneration).

5.2. Dysoxia and dissolved Cr

O_2-depleted waters are known to influence [Cr], redox speciation, and $\delta^{53}Cr$ (Murray et al., 1983; Rue et al., 1997; Davidson et al., 2020; Moos et al., 2020; Nasemann et al., 2020; Huang et al., 2021; Janssen et al., 2022). In these environments, Cr(III) can be the dominant oxidative state of Cr, and local [Cr] minima are related to the removal of reactive Cr(III) (e.g., Murray et al., 1983; Rue et al., 1997; Davidson et al., 2020; Huang et al., 2021). The reduction of Cr and its subsequent removal onto sinking particles induce an isotope fractionation due to the preferential reduction and scavenging of isotopically light Cr as Cr(III), leading to isotopically heavier residual seawater (e.g., Zink et al., 2010; Wanner and Sonnenthal, 2013; Davidson et al., 2020; Huang et al., 2021). Chromium removal in O_2-depleted water can be due to reduction and removal within the water column in the open ocean (e.g., Murray et al., 1983; Rue et al., 1997; Moos et al., 2020; Huang et al., 2021), or to removal within reducing sediments (e.g., Moos et al., 2020).

In comparing O_2-depleted (yet not anoxic) waters throughout the

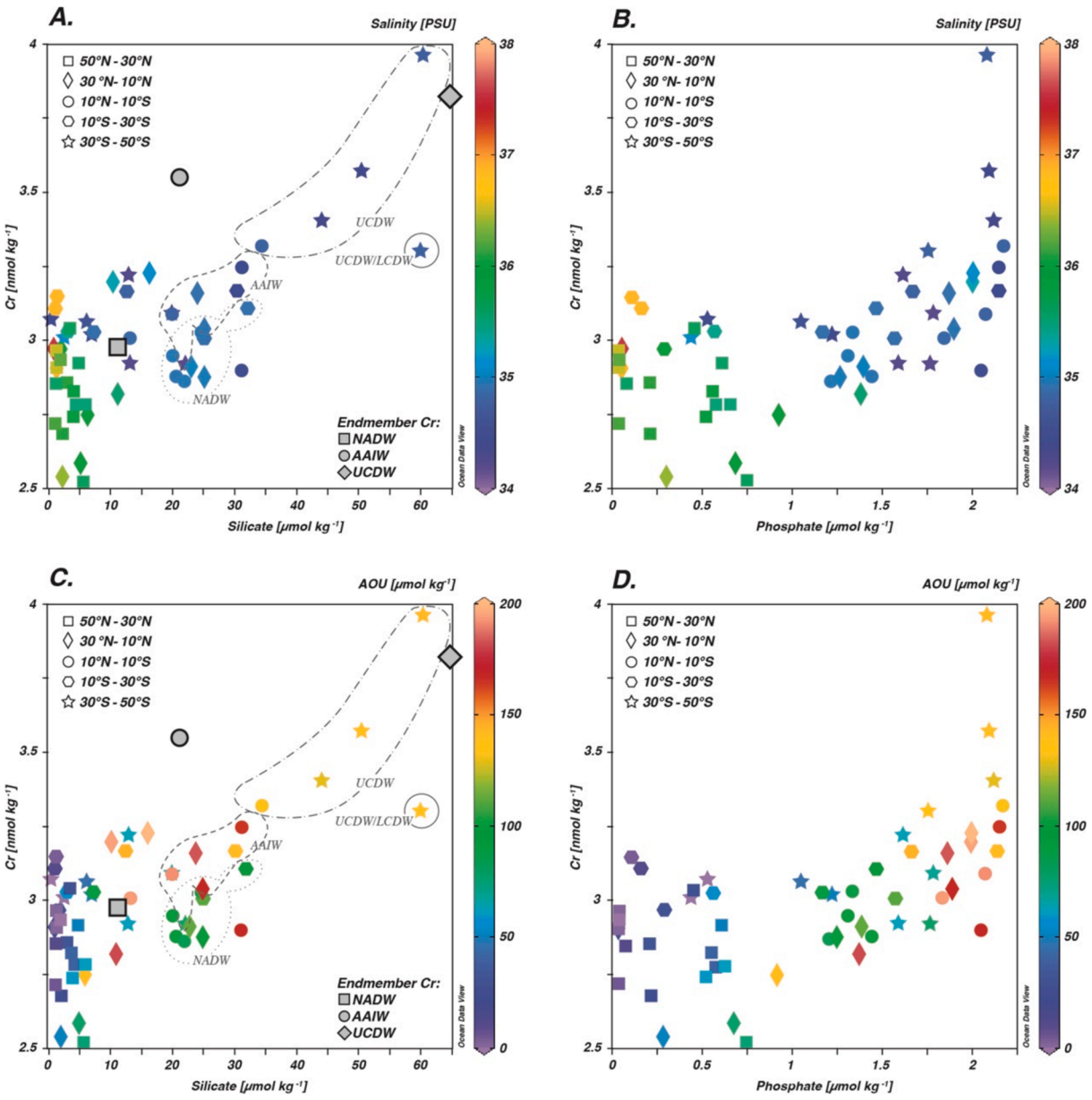

Fig. 6. [Cr] against silicate (Si) concentration (left column) and phosphate (PO_4^{3-}), concentration (right column) compared with salinity (top graphs A and B) and AOU (bottom graphs C and D) in z axis originate from WOA 2018. The symbols correspond to latitude ranges (see legend): squares correspond to stations 3, 7, 10, diamonds correspond to stations 17, 23, and 26, circles correspond to stations 33 and 40, hexagons correspond to stations 45 and 50, and stars correspond to stations 60 and 62. Shallow water (0 to 150 m) data at lower latitude (20 °S to 20 °N) were excluded from the figure to better visualize the main water masses. The grey symbols indicate Cr endmembers: NADW values defined using data from (Baconnais, 2022), while AAIW and UCDW values are based on (Janssen et al., 2021). Additional details of this figure are available in Figure S2 and Figure S3.

global ocean where Cr removal is apparent, a threshold around ~10 µmol l^{-1} O_2 has been noted, above which Cr reduction and removal has not been reported (Goring-Harford et al., 2018; Moos and Boyle, 2019, Janssen et al., 2020, Nasemann et al., 2020; Wang et al., 2023a). Instead, Cr depletion and associated isotope fractionation is restricted to lower [O_2] (Nasemann et al., 2020; Moos et al., 2020; Huang et al., 2021). AMT 29 encompasses O_2-depleted waters between 10 °S and 18 °N (Figs. 2 and 3), with ambient [O_2] remaining ≥47 µmol l^{-1} (Fig. 2). Both [Cr] and δ^{53}Cr profiles within and outside of the OMZ are comparable (Fig. 3, Table 1), indicating negligible Cr removal in these environments. This is most likely explained by O_2 levels being insufficiently low to drive substantial Cr reduction and affect Cr distributions, both along the transect and within much of the Atlantic. Similar observations have been made in the tropical North Atlantic (Goring-Harford et al., 2018; Wang et al., 2023a), as well as at comparable or lower [O_2] in the North Pacific (Murray et al., 1983; Moos and Boyle, 2019; Janssen et al., 2020).

5.3. Biological pump

The removal of Cr by phytoplankton is considered to impact Cr distribution by scavenging reactive Cr(III), which is typically enriched in ^{52}Cr and leads to a relatively high residual δ^{53}Cr (e.g., Achterberg and Van Den Berg, 1997; Scheiderich et al., 2015; Semeniuk et al., 2016; Janssen et al., 2020). For instance, in the North Pacific, elevated net community productivity corresponds to [Cr] depletion and relatively lower δ^{53}Cr values compared to less productive ecosystems (Janssen et al., 2020). The influence of biological activity on the distribution of Cr

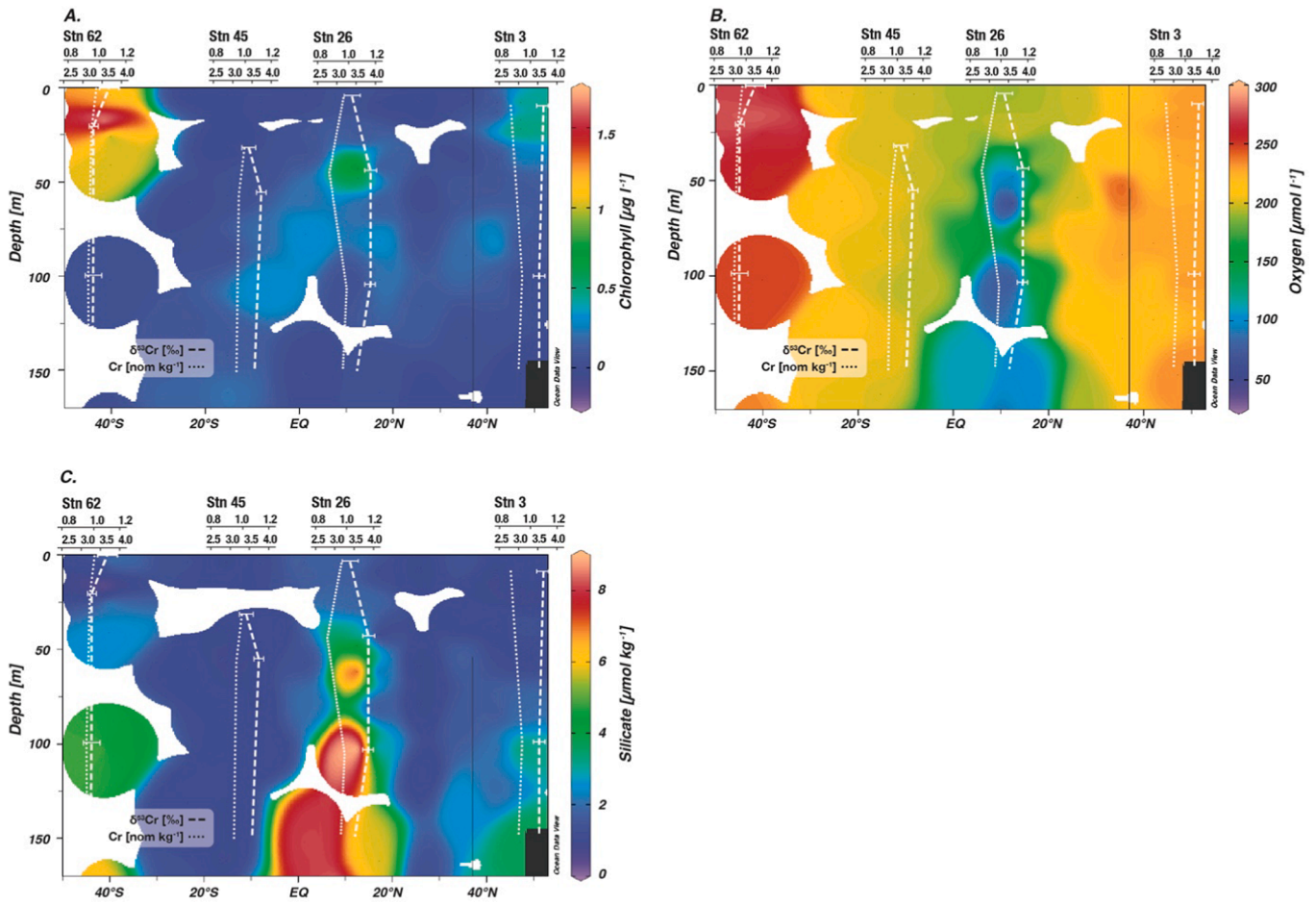

Fig. 7. AMT 29 section in shallow water (150 m) for a. Chlorophyll [µg l^{-1}], b. Oxygen [µmol l^{-1}], c. Silicate [µmol l^{-1}], and overlapping δ^{53}Cr (dashed white line) and [Cr] (dotted white line). The stations were selected due to their available data in shallow water.

along AMT29 is subtle (Table 1 and Fig. 3) and therefore, requires cautious interpretation. The highest chlorophyll concentration (maximum 1.75 µg l^{-1}) was observed at the southernmost stations 62 and 60, around 25 m (Fig. 7A). Cr levels at stations 62 and 60 (Fig. 7A, Table 1) did not significantly differ from stations characterized by lower chlorophyll concentrations (Fig. 7A and Table 1). However, at station 26, a small correlation between Cr and chlorophyll concentration was observed at 43 m, where [Cr] show a slight depletion and δ^{53}Cr exhibits a slight enrichment (+0.08 ± 0.03 ‰ 2SEM) within the subsurface chlorophyll maximum compared to the water above. At station 3, a small correlation between [Cr] and chlorophyll concentration is noted, with [Cr] depletion of 0.19 nmol kg^{-1} from 17 to 103 m, while δ^{53}Cr remains constant. While subtle signals may be present in these stations, δ^{53}Cr and [Cr] signals are close to the limits of analytical precision. Therefore, there is a lack of clear signals of biological productivity impacting Cr, similar to previous observations in the subtropical Atlantic (Goring-Harford et al., 2018) and (Wang et al., 2023a). The lack of this clear signal impacting Cr is probably due to generally reduced biological productivity in the Atlantic basin at these latitudes (e.g., Berger et al., 1989; Sigman and Hain, 2012), as well as the comparatively larger impact of other processes such as mixing.

6. Conclusion

Our study sheds light on the complex dynamics of [Cr] and δ^{53}C distribution in the upper ~2000 m of the Atlantic Ocean, along AMT 29. We investigated the influence of oxygen levels and biological activity on Cr cycling, finding limited evidence of their impact. Instead, our study supports the notion that, similar to other trace metals in the Atlantic, the main mechanism responsible for basin-scale Cr distributions relate to horizontal advection and water mass mixing. In general, in the Atlantic Ocean, [Cr] increase southwards while δ^{53}C decreases, consistent with control from horizontal advection and mixing with more Cr-rich water masses originating from the Southern Ocean. Therefore, deep water Cr distributions largely reflect the interweaving of southward-propagating NADW and northward-propagating AAIW and UCDW. Similarly, Cr and macronutrient relationships correspond with gradients in water masses and transitions between these waters, rather than directly coupled, vertically-driven processes. The importance of mixing results in a weak correlation between δ^{53}Cr and Ln([Cr]) complicates the closed-system assumption of the Rayleigh model which underscores the necessity of considering mixing processes in interpreting Cr data.

Overall, this study highlights the nuanced nature of Cr behavior in the ocean and underscores the importance of mixing in shaping distributions, which has implications for the use of Cr as a paleoproxy (e.g., for tracing past oxygenation events). In the future studies, the use of Cr and δ^{53}Cr as biogeochemical tracers through time should therefore consider potential impacts from mixing, which can drive deviations from closed system Rayleigh fractionation trends.

Author contributions

Samples were collected by NS. Most of chromium purification was performed by NS and most analyses were performed by DJ. Replicates and additional measurements were conducted by DG. DG wrote the first draft of the manuscript. All authors contributed to the interpretation of

the data and preparation of the final manuscript.

Declaration of AI and AI-assisted technologies in the writing process

During the preparation of this work DG used ChatGPT to improve readability and language. After using this tool, DG reviewed and edited the content as needed and takes full responsibility for the content of the publication.

Data availability

All new Cr concentration, its stable isotopes, and hydrographic data are archived on Zenodo (Zenodo https://doi.org/10.5281/zenodo.11093009). Hydrographic data are also available on the AMT 29 cruise report (Dall'Olmo et al., 2020). Phosphate, silicate, oxygen, and salinity data used in Fig. 2 and salinity used in Fig. 5 are available on World Ocean Atlas WOA 2018.

CRediT authorship contribution statement

D. Gilliard: Writing – original draft, Data curation. **D.J. Janssen:** Supervision, Formal analysis. **N. Schuback:** Formal analysis. **S.L. Jaccard:** Supervision.

Declaration of competing interest

The authors declare that they have no known competing financial interests or personal relationships that could have appeared to influence the work reported in this paper.

Acknowledgements

We are grateful to principal scientist Dr. Giorgio Dall'Olmo and the captain and crew of RRS Discovery for their support during the work at sea. The Atlantic Meridional Transect is funded by the UK Natural Environment Research Council through its National Capability Long-term Single Centre Science Programme, Climate Linked Atlantic Sector Science (grant number NE/R015953/1). The Atlantic Meridional Transect is funded by the UK Natural Environment Research Council through its National Capability Long-term Single Centre Science Programme, Climate Linked Atlantic Sector Science (grant number NE/R015953/1). This study contributes to the international IMBeR project and is contribution number 411 of the AMT programme. We thank Malcolm Woodward and Rebecca May for nutrients data and Rebecca May for oxygen measurements. We would like to express our gratitude to associate editor Prof. Tim Conway and three anonymous reviewers for their insightful suggestions and constructive criticisms, which greatly improved the manuscript. The study was funded by a European Research Council (ERC) Consolidator Grant (SCrIPT, grant agreement 819139) to SLJ. The Cr data obtained at UNIL were analyzed on a Neptune MC-ICP-MS acquired with funds supported in part by SNSF grant 206021_2055399. We thank Isabelle Baconnais, Patrick Blaser, and Sylvie Bruggmann for the time they provided in sharing their knowledge in oceanography and geochemistry.

Appendix A. Supplementary material

The supplementary section contains two tables and three figures. The first table lists OSIL measurements, and the second table includes data replicates. The first figure summarizes [Cr] in the Atlantic Ocean in a data compilation. The second and third figures examine the relationship between [Cr] and macronutrients, salinity, and PSU within specific water masses from AMT29 and Cr endmember data for NADW, UCDW, and AAIW. Supplementary material to this article can be found online at https://doi.org/10.1016/j.gca.2024.10.017.

References

Achterberg, E.P., van den Berg, C.M.G., 1997. Chemical speciation of chromium and nickel in the western Mediterranean. Deep-Sea Res. II 44, 693–720.
Baconnais, I., 2022. A study of the geochemistry of chromium isotopes in the modern oceans. University of Saskatchewan. Doctoral dissertation.
Ball, J.W., Bassett, R.L., 2000. Ion exchange separation of chromium from natural water matrix for stable isotope mass spectrometric analysis. Chem. Geol. 168, 123–134.
Berger, W.H., Smetacek, V.S., Wefer, G., 1989. Ocean productivity and paleoproductivity-an overview. In: Berger, W.H., Smetacek, V.S., Wefer, G. (Eds.), Productivity of the Ocean: Present and past. Wiley, Chichester, pp. 1–34.
Bianchi, A.A., Giulivi, C.F., Piola, A.R., 1993. Mixing in the Brazil-Malvinas confluence. Deep Sea Res. Oceanogr. Res. Pap. 40 (7), 1345–1358.
Blanke, B., Arhan, M., Speich, S., 2006. Salinity changes along the upper limb of the Atlantic thermohaline circulation. Geophys. Res. Lett. 33.
Bonnand, P., James, R.H., Parkinson, I.J., Connelly, D.P., Fairchild, I.J., 2013. The chromium isotopic composition of seawater and marine carbonates. Earth. Planet. Sci. Let. 382, 10–20.
Bruggmann, S., Severmann, S., McManus, J., 2023. Geochemical conditions regulating chromium preservation in marine sediments. Geochim. Cosmochim. Acta 348, 239–257.
Bruland, K.W., Middag, R., Lohan, M.C., 2014. Controls of Trace Metals in Seawater, 2nd ed. Elsevier Ltd.
Brzezinski, M.A., Jones, J.L., 2015. Coupling of the distribution of silicon isotopes to the meridional overturning circulation of the North Atlantic Ocean. Deep-Sea Res. II 116, 79–88.
Campbell, J.A., Yeats, P.A., 1981. Dissolved chromium in the northwest Atlantic Ocean. Earth. Planet. Sci. Let. 53, 427–433.
Chen, X.-G., Gledhill, M., Lohan, M.C., Milne, A., Achterberg, E.P., 2024. Surface ocean biogeochemistry and deep ocean circulation control relationships between nutrient-type trace metals (Cd, Ni, Cu, and Zn) and nutrients in the South Atlantic Ocean near the subtropical front. Geochim. Cosmochim. Acta 370, 144–160.
Connelly, D.P., Statham, P.J., Knap, A.H., 2006. Seasonal changes in speciation of dissolved chromium in the surface Sargasso Sea. Deep Sea Res. Part I 53, 1975–1988.
Conway, T.M., John, S.G., 2015. Biogeochemical cycling of cadmium isotopes along a high-resolution section through the North Atlantic Ocean. Geochim. Cosmochim. Acta 148, 269–283.
Cranston, R.E., 1983. Chromium in Cascadia Basin, northeast Pacific Ocean. Mar. Chem. 13, 109–125.
D'Arcy, J., Babechuk, M.G., Døssing, L.N., Gaucher, C., Frei, R., 2016. Processes controlling the chromium isotopic composition of river water: Constraints from basaltic river catchments. Geochim. Cosmochim. Acta 186, 296–315.
Dall'Olmo, G., 2020. AMT29 Cruise Report, https://www.plymsea.ac.uk/id/eprint/9524/.
Davidson, A.B., Semeniuk, D.M., Koh, J., Holmden, C., Jaccard, S.L., Francois, R., Crowe, S.A., 2020. A Mg(OH)2 coprecipitation method for determining chromium speciation and isotopic composition in seawater. Limnol. Oceanogr. Meth. 18, 8–19.
Eary, L.E., Rai, D., 1987. Kinetics of Chromium (III) Oxidation to Chromium (VI) by Reaction with Manganese Dioxide. Environ. Sci. Tech. 21, 1187–1193.
Elderfield, H., 1970. Chromium in sea water. Earth. Planet. Sci. Let. 9, 10–16.
Ellwood, M.J., Bowie, A.R., Baker, A., Gault-Ringold, M., Hassler, C., Law, C.S., Maher, W.A., Mariner, A., Nodder, S., Sander, S., Stevens, C., Townsend, A., van der Merwe, P., Woodward, E.M.S., Wuttig, K., Boyd, P., 2018. Insights into the biogeochemical cycling of iron, nitrate, and phosphate across a 5,300 km South Pacific zonal section (153E–150W). Global Biogeochem Cy 32, 187–207.
Emery, W.J., 2003. Water types and water masses. Ocean Circulation. Science 1979, 1556–1567.
Frei, R., Gaucher, C., Poulton, S.W., Canfield, D.E., 2009. Fluctuations in Precambrian atmospheric oxygenation recorded by chromium isotopes. Nature 461, 250–254.
Frei, R., Gaucher, C., Døssing, L.N., Sial, A.N., 2011. Chromium isotopes in carbonates - A tracer for climate change and for reconstructing the redox state of ancient seawater. Earth. Planet. Sci. Let. 312, 114–125.
Frei, R., Xu, L., Frederiksen, J.A., Lehmann, B., 2021. Signals of combined chromium–cadmium isotopes in basin waters of the Early Cambrian –_Results from the Maoshi and Zhijin sections, Yangtze Platform, South China. Chem. Geol. 563, 120061.
Garcia, H.E., Boyer, T.P., Baranova, O.K., Locarnini, R.A., Mishonov, A.V., Grodsky, A.E., Zweng, M.M., 2019. World ocean atlas 2018: Product documentation. A. Mishonov, Technical Editor.
George, E., Stirling, C.H., Gault-Ringold, M., Ellwood, M.J., Middag, R., 2019. Marine biogeochemical cycling of cadmium and cadmium isotopes in the extreme nutrient-depleted subtropical gyre of the South West Pacific Ocean. Earth Planet. Sci. Let. 514, 84–95.
Goring-Harford, H.J., Klar, J.K., Pearce, C.R., Connelly, D.P., Achterberg, E.P., James, R. H., 2018. Behaviour of chromium isotopes in the eastern sub-tropical Atlantic Oxygen Minimum Zone. Geochim. Cosmochim. Acta 236, 41–59.
Holmden, C., Jacobson, A.D., Sageman, B.B., Hurtgen, M.T., 2016. Response of the Cr isotope proxy to Cretaceous Ocean Anoxic Event 2 in a pelagic carbonate succession from the Western Interior Seaway. Geochim Cosmochim Acta 186, 277–295.
Horner, T.J., Little, S.H., Conway, T.M., Farmer, J.R., Hertzberg, J.E., Janssen, D.J., Lough, A.J.M., McKay, J.L., Tessin, A., Galer, S.J.G., Jaccard, S.L., Lacan, F., Paytan, A., Wuttig, K., GEOTRACES-PAGES Biological Productivity Working Group Members, 2021. Bioactive trace metals and their isotopes as paleoproductivity proxies: An assessment using GEOTRACES-era data. Glob. Biogeochem. Cy. 35 (11). e2020GB006814.

Huang, T., Moos, S.B., Boyle, E.A., 2021. Trivalent chromium isotopes in the eastern tropical North Pacific oxygen-deficient zone. Proc. Nat. Acad. Sci. USA 118 (8).
Janssen, D.J., Rickli, J., Quay, P.D., White, A.E., Nasemann, P., Jaccard, S.L., 2020. Biological control of chromium redox and stable isotope composition in the surface ocean. Glob. Biogeochem. Cy. 34, e2019GB006397.
Janssen, D.J., Rickli, J., Abbott, A.N., Ellwood, M.J., Twining, B.S., Ohnemus, D.C., Nasemann, P., Gilliard, D., Jaccard, S.L., 2021. Release from biogenic particles, benthic fluxes, and deep water circulation control Cr and d53Cr distributions in the ocean interior. Earth. Planet. Sci. Let. 574, 117163.
Janssen, D.J., Gilliard, D., Rickli, J., Nasemann, P., Koschinsky, A., Hassler, C.S., Bowie, A.R., Ellwood, M.J., Kleint, C., Jaccard, S.L., 2023. Chromium stable isotope distributions in the southwest Pacific Ocean and constraints on hydrothermal input from the Kermadec Arc. Geochim. Cosmochim. Acta 342, 31–44.
Janssen, D.J., Rickli, J., Wille, M., Sepulveda, S.O., Vogel, H., Dellwig, O., Berg, J.S., Bouffard, D., Lever, M.A., Hassler, C.S., Jaccard, S.L., 2022. Chromium cycling in Redox-stratified basins challenges d53Cr paleoredox proxy applications. Geophys. Res. Lett. 49.
Jeandel, C., Minster, J.F., 1987. Chromium behavior in the ocean: global versus regional processes. Glob. Biogeochem. Cy. 1, 131–154.
Liu, M., Tanhua, T., 2021. Water masses in the Atlantic Ocean: characteristics and distributions. Ocean Sci. 17, 463–486.
McClain, C.N., Maher, K., 2016. Chromium fluxes and speciation in ultramafic catchments and global rivers. Chem. Geol. 426, 135–157.
Middag, R., de Baar, H.J.W., Bruland, K.W., 2019. The relationships between dissolved zinc and major nutrients phosphate and silicate along the GEOTRACES GA02 transect in the West Atlantic Ocean. Glob. Biogeochem. Cy. 33, 63–84.
Milletto, M., Wang, X., Planavsky, N.J., Luther, G.W., Lyons, T.W., Tebo, B.M., 2021. Marine microbial Mn(II) oxidation mediates Cr(III) oxidation and isotope fractionation. Geochim. Cosmochim. Acta 297, 101–119.
Moos, S.B., 2018. The marine biogeochemistry of chromium isotopes. Massachusetts Institute of Technology. Doctoral dissertation.
Moos, S.B., Boyle, E.A., 2019. Determination of accurate and precise chromium isotope ratios in seawater samples by MC-ICP-MS illustrated by analysis of SAFe Station in the North Pacific Ocean. Chem. Geol. 511, 481–493.
Moos, S.B., Boyle, E.A., Altabet, M.A., Bourbonnais, A., 2020. Investigating the cycling of chromium in the oxygen deficient waters of the Eastern Tropical North Pacific and the Santa Barbara Basin using stable isotopes. Mar. Chem. 221, 103756.
Murray, J.W., Spell, B., Paul, B., 1983. The contrasting geochemistry of manganese and chromium in the eastern tropical Pacific Ocean. In: Wong C.S., Boyle E., Bruland K. W., Burton J.D., Goldberg E.D. (eds) Trace Metals in Sea Water. NATO Conference Series (IV Marine Sciences), 9. Springer, Boston, MA, pp. 643–669.
Nasemann, P., Janssen, D.J., Rickli, J., Grasse, P., Franck, M., Jaccard, S.L., 2020. Chromium reduction and associated stable isotope fractionation restricted to anoxic shelf waters in the Peruvian Oxygen Minimum Zone. Geochim. Cosmochim. Acta 285, 207–224.
Planavsky, N.J., Cole, D.B., Isson, T.T., Reinhard, C.T., Crockford, P.W., Sheldon, N.D., Lyons, T.W., 2018. A case for low atmospheric oxygen levels during Earth's middle history. Emerg. Top. Life. Sci. 2, 149–159.
Pöppelmeier, F., Janssen, D.J., Jaccard, S.L., Stocker, T.F., 2021. Modeling the marine chromium cycle: new constraints on global-scale processes. Biogeosciences 18 (19), 5447–5463.
Ramjuttun, R., 1997. The chemical speciation of chromium in seawater by cathodic stripping voltammetry. Memorial University of Newfoundland. Doctoral dissertation.
Reinhard, C.T., Planavsky, N.J., Wang, X., Fischer, W.W., Johnson, T.M., Lyons, T.W., 2014. The isotopic composition of authigenic chromium in anoxic marine sediments: A case study from the Cariaco Basin. Earth Planet. Sci. Let. 407, 9–18.
Rickli, J., Janssen, D.J., Hassler, C., Ellwood, M.J., Jaccard, S.L., 2019. Chromium biogeochemistry and stable isotope distribution in the Southern Ocean. Geochim. Cosmochim. Acta 262, 188–206.
Rue, E.L., Smith, G.J., Cutter, G.A., Bruland, K.W., 1997. The response of trace element redox couples to suboxic conditions in the water column. Deep Sea Res. i. 44 (1), 113–134.
Saager, P.M., de Baar, H.J.W., de Jong, J.T.M., Nolting, R.F., Schijf, J., 1997. Hydrography and local sources of dissolved trace metals Mn, Ni, Cu and Cd in the northeast Atlantic Ocean. Mar. Chem. 57, 195–216.
Sarmiento, J.L., Gruber, N., Brzezinski, M.A., Dunne, J.P., 2004. High-latitude controls of thermocline nutrients and low latitude biological productivity. Nature 427, 56–60.
Sarmiento, J.L., Simeon, J., Gnanadesikan, A., Gruber, N., Key, R.M., Schlitzer, R., 2007. Deep ocean biogeochemistry of silicic acid and nitrate. Glob. Biogeochem. Cy. 21 (1).
Scheiderich, K., Amini, M., Holmden, C., Francois, R., 2015. Global variability of chromium isotopes in seawater demonstrated by Pacific, Atlantic, and Arctic Ocean samples. Earth Planet. Sci. Lett. 423, 87–97.
Schlitzer, Reiner, Ocean Data View, https://odv.awi.de, (2023).
Schoenberg, R., Zink, S., Staubwasser, M., von Blanckenburg, F., 2008. The stable Cr isotope inventory of solid Earth reservoirs determined by double spike MC-ICPMS. Chem. Geol. 249, 294–306.
Semeniuk, D.M., Maldonado, M.T., Jaccard, S.L., 2016. Chromium uptake and adsorption in marine phytoplankton – Implications for the marine chromium cycle. Geochim. Cosmochim. Acta 184, 41–54.
Sherrell, R.M., Boyle, E.A., 1988. Zinc, chromium, vanadium and iron in the Mediterranean Sea. Deep Sea Res. Part A. Oceanogr. Res. Pap., 35 1988, pp. 1319-1334.
Sigman, D.M., Hain, M.P., 2012. The biological productivity of the ocean. Nature Education Knowl. 3, 21.
Steiner, Z., Antler, G., Berelson, W.M., Crockford, P.W., Dunlea, A.G., Hou, Y., Adkins, J. F., Turchyn, A.V., Achterberg, E.P., 2023. Trace Element Geochemistry in North Pacific Red Clay Sediment Porewaters and Implications for Water-Column Studies. Global Biogeochem. Cy. 37 (11).
Stramma, L., England, M., 1999. On the water masses and mean circulation of the South Atlantic Ocean. J. Geophys. Res. 104, 20863–20883.
Sunda, W.G., Huntsman, S.A., 2000. Effect of Zn, Mn, and Fe on Cd accumulation in phytoplankton: Implications for oceanic Cd cycling. Limnol Oceanogr 45, 1501–1516.
Talley, L.D., 2011. Descriptive physical oceanography: an introduction. Academic press.
Tomczak, M. and Godfrey, J., 2003. Regional Oceanography: An introduction. 2nd Edition, Daya Publishing House.
Tyson, R.V., Pearson, T.H., 1991. Modern and ancient continental shelf anoxia: an overview. In Modern and Ancient Continental Shelf Anoxia (eds. R. V. Tyson and T. H. Pearson). Geol. Soc. London Sp. Publ. 58, 1–24.
Vance, D., Little, S.H., de Souza, G.F., Khatiwala, S., Lohan, M.C., Middag, R., 2017. Silicon and zinc biogeochemical cycles coupled through the Southern Ocean. Nat. Geosci. 10, 202–206.
Wang, X., Glass, J.B., Reinhard, C.T., Planavsky, N.J., 2019. Species-dependent chromium isotope fractionation across the eastern tropical north pacific oxygen minimum zone. Geochem. Geosyst. 20, 2499–2514.
Wang, W., Goring-Harford, H., Kunde, K., Woodward, E.M.S., Lohan, M.C., Connelly, D. P., James, R.H., 2023a. Biogeochemical cycling of chromium and chromium isotopes in the sub-tropical North Atlantic Ocean. Front. Mar. Sci. 10, 1165304.
Wang, W., Lough, A.J.M., Goring-Harford, H., Flanagan, O., Gonzales-Santana, D., Resing, J., Connelly, D., Lohan, M.C., Tagliabue, A., James, R.H., 2023b. Fractionation of iron and chromium isotopes in hydrothermal plumes from the northern Mid-Atlantic Ridge. Earth. Planet. Sci. Let. 624, 118468.
Wanner, C., Sonnenthal, E.L., 2013. Assessing the control on the effective kinetic Cr isotope fractionation factor: A reactive transport modeling approach. Chem. Geol. 337–338, 88–98.
Wei, W., Klaebe, R., Ling, H.-F., Huang, F., Frei, R., 2020. Biogeochemical cycle of chromium isotopes at the modern Earth's surface and its applications as a paleo-environment proxy. Chem. Geol. 541, 119570.
Wu, J., Roshan, S., Chen, G., 2014. The distribution of dissolved manganese in the tropical-subtropical North Atlantic during US GEOTRACES 2010 and 2011 cruises. Mar. Chem. 166, 9–24.
Wyatt, N.J., Milne, A., Woodward, E.M.S., Rees, A.P., Browning, T.J., Bouman, H.A., Worsfold, P.J., Lohan, M.C., 2014. Biogeochemical cycling of dissolved zinc along the GEOTRACES South Atlantic transect GA10 at 40∘S. Glob. Biogeochem. Cycles 28, 44–56.
Yamakawa, A., Yamashita, K., Makishima, A., Nakamura, E., 2009. Chemical separation and mass spectrometry of Cr, Fe, Ni, Zn, and Cu in Terrestrial and extraterrestrial materials using thermal ionization mass spectrometry. Anal. Chem. 81 (23), 9787–9794.
Zink, S., Schoenberg, R., Staubwasser, M., 2010. Isotopic fractionation and reaction kinetics between Cr(III) and Cr(VI) in aqueous media. Geochim. Cosmochim. Acta 74 (20).